Journal of Power Sources 187 (2009) 261–267

Contents lists available at ScienceDirect

Journal of Power Sources

journal homepage: www.elsevier.com/locate/jpowsour

Selective micro-etching of duplex stainless steel for preparing manganese oxide supercapacitor electrode

Szu-Jung Pan, Yi-Ju Shih, Jhen-Rong Chen, Jeng-Kuei Chang, Wen-Ta Tsai*

Department of Materials Science and Engineering, National Cheng Kung University, 1 University Road,Tainan 701, Taiwan

ARTICLE INFO

Article history:
Received 23 June 2008
Received in revised form 3 September 2008
Accepted 25 October 2008
Available online 8 November 2008

Keywords:
Selective dissolution
Micro-etching
Duplex stainless steel
Manganese oxide
Supercapacitor

ABSTRACT

In this investigation, manganese oxide electrodes that incorporate selectively micro-etched duplex stainless steel (DSS) for supercapacitor applications were fabricated. The experimental results demonstrate that selective dissolution of the γ phase could result in the formation of α phase network, and vice versa. Controlling the extent of selective dissolution produces a surface with a concave–convex morphology, increasing the surface area. Manganese oxide could then be anodically deposited onto the etched dual phase steel current collector. The experimental results of cyclic voltammetry (CV) show that the specific capacitance increased with the etching depth of either the γ or the α phase. Additionally, selective dissolution occurred in α phase had a better effect on increasing the specific capacitance. The successful application of selective dissolution in fabricating a current collector was thus demonstrated.

1. Introduction

The charge storage capacity of a supercapacitor can be improved by increasing the electrode surface area. For a manganese oxide supercapacitor, the oxide film can be deposited on many substrates, which act as current collectors. Along with graphite [1–3], nickel [4,5] and other conductive materials [6,7], stainless steel can be used because it is inert in various supercapacitor electrolytes. Among the various grades of stainless steel, duplex stainless steels (DSSs) with a relatively high Cr content are particularly attractive because of their higher corrosion resistance in such electrolytes as KOH, Na_2SO_4 solutions and others.

DSS comprises austenitic (γ) and ferritic (α) phases. The former has a face-centered cubic (FCC) crystal structure while the latter is body-centered cubic (BCC). Each phase has a specific chemical composition, and therefore manifests a distinct electrochemical nature in certain electrolytes. Previous studies have demonstrated that the mixed H_2SO_4/HCl solutions yield two anodic peaks in the active-to-passive transition region of the potentiodynamic polarization curves of 2205 DSS. Selective (preferential) dissolution can occur at each of these characteristic potentials [8]. Accordingly, Tsai and Chen developed a novel procedure that involves selective micro-etching reaction for fabricating micro-networks or rods with an exclusively γ or α phase from dual-phase stainless steel [9]. After one of the constituent phases is selectively dissolved in a specific mixed H_2SO_4/HCl solution, the concave/convex microstructure of a dual-phase stainless steel can give rise to an increase in surface area. This etched stainless steel may be advantageous for use as an electrode substrate for supercapacitor applications.

Manganese oxide has been found to be a promising substitute for ruthenium oxide as the electrode material for supercapacitors [10,11]. It can be anodically deposited under either constant potential [12] or constant current [13] conditions, to prepare a supercapacitor electrode using graphite or nickel substrate. The use of a substrate with a high specific surface area is considered to increase the specific capacitance of a manganese oxide electrode (in terms of $F\,g^{-1}$). Coating manganese oxide onto a stainless steel substrate with a concave/convex feature, as presented in Fig. 1, may yield a high specific capacitance. Therefore, this investigation examines the feasibility of increasing the specific capacitance of a manganese oxide electrode by the selective micro-etching of a DSS substrate.

2. Experimental

2.1. Specimen preparation

Table 1 presents the chemical composition of the 2205 DSS rod used in this study. After solid solution heat treatment at 1100 °C for 30 min, the α/γ volume ratio was approximately 1.13, where α was the continuous phase. Table 1 also presents the respective

* Corresponding author. Tel.: +886 6 2757575x62927; fax: +886 6 2754395.
E-mail address: wttsai@mail.ncku.edu.tw (W.-T. Tsai).

0378-7753/$ – see front matter © 2008 Elsevier B.V. All rights reserved.
doi:10.1016/j.jpowsour.2008.10.122

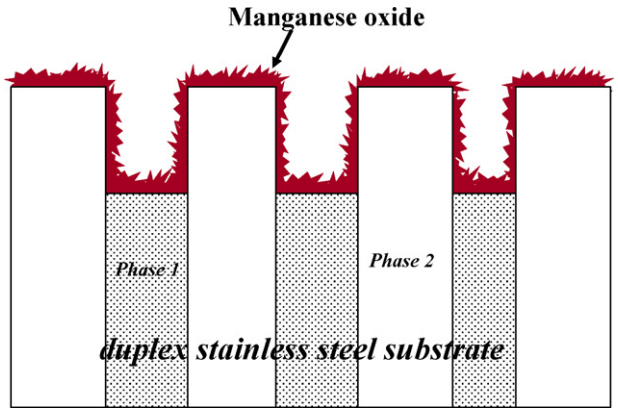

Fig. 1. Schematic diagram showing the cross-sectional feature of a selectively etched 2205 DSS coated with manganese oxide.

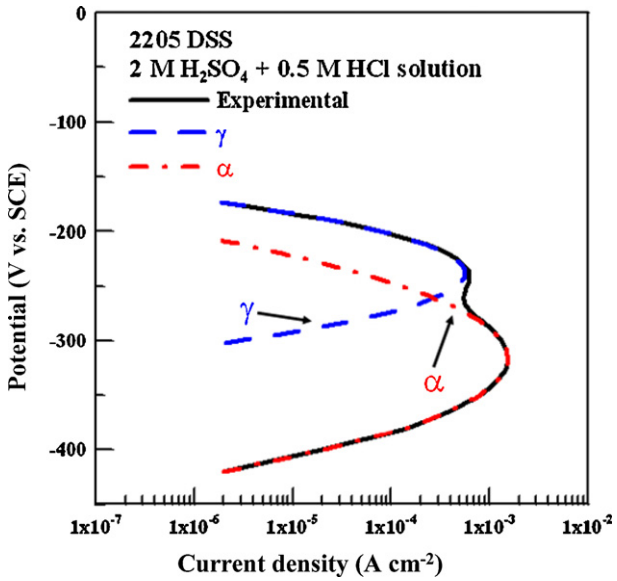

Fig. 2. Full and dissociated potentiodynamic polarization curves of the active-to-passive transition region of 2205 DSS in mixed 2 M H_2SO_4 + 0.5 M HCl solution.

chemical compositions of α and γ phases, analyzed by energy dispersive spectrometry (EDS). The solution heat-treated steel rod was then cut into a 2 mm-thick disc with a cross-sectional area of 1 cm × 1 cm. This disc was connected to a copper wire, and mounted in epoxy resin, before being ground using SiC paper to a grit finish of #1000. Finally, the mounted specimen was cleaned ultrasonically in distilled water before selective etching and manganese oxide coating.

2.2. Selective etching

A mixed 2 M H_2SO_4 + 0.5 M HCl solution was adopted herein. The etching potentials were determined from the potentiodynamic polarization curve of 2205 DSS. The procedure for measuring the electrochemical polarization curve has been elucidated elsewhere [9]. Fig. 2 plots the potentiodynamic polarization curve in the active-to-passive transition region of 2205 DSS in mixed 2 M H_2SO_4 + 0.5 M HCl solution. The polarization curve can be dissociated into two distinct curves one for the γ phase and the other for α phase as presented in Fig. 2. The respective characteristic peak potentials, −260 and −320 mV (with respect to a saturated calomel electrode, SCE), were selected for potentiostatic etching of the γ and α phases, respectively. The etching time varied from 1 to 4 h. The specimens designated as A1, A2, and A4 were those of 2205 DSS etched at the characteristic potential for selective dissolution of the γ phase for 1, 2 and 4 h, respectively. Specimen A0 was not etched. Similarly, the specimens F0, F1, F2 and F4 were those with α phase selectively dissolved.

2.3. Anodic deposition of manganese oxide

Manganese oxide was electroplated onto each of the various etched 2205 DSS substrates by anodic deposition in a neutral 0.25 M $MnSO_4$ plating solution at room temperature. Anodic deposition was performed in a three-electrode system at a constant applied potential, as reported upon elsewhere [14,15]. During the deposition, the substrate was held as the anode while a platinum sheet and an SCE were used as the counter electrode and the reference electrode, respectively. An EG&G Princeton Applied Research model 263 potentiostat was adopted to apply a total charge of 0.2 C at a constant potential of 0.9 V. After electrodeposition, the electrode was dried in air.

2.4. Cyclic voltammetry

The supercapacitive behavior of the manganese oxide electrode was characterized by cyclic voltammetry (CV) in 0.1 M Na_2SO_4 solution at room temperature. The test cell was a three-electrode system of which the manganese oxide electrode was the working electrode. A platinum sheet and an SCE were used as the counter electrode and the reference electrode, respectively. The measuring instrument was an Autolab PGSTAT302 potentiostat. The potential was scanned in a potential range of 0–1 V. The CV scan rate was varied from 5 to 100 mV s^{-1}.

2.5. Surface morphology and chemical state analyses

The surface morphologies and cross-section images of etched 2205 DSS and those coated with manganese oxide were examined with a scanning electron microscope (SEM). X-ray photoelectron spectroscopy (XPS) was adopted to analyze the chemical state of the manganese oxides. The measurements were made using an ESCA 210 (VG Science Ltd.) spectrometer. Monochromatic Al Kα (1486.6 eV) radiation was the X-ray source. The pressure in the analyzing chamber was about 1 × 10^{-9} Torr during the measurement.

Table 1
Chemical compositions (in wt.%) of 2205 DSS and the constituent ferritic (α) and austenitic (γ) phases.

Element	Fe	Cr	Ni	Mo	Mn	Si	C	Cu	P	S	N
2205 DSS	Bal.	22.4	5.42	3.24	1.43	0.41	0.014	0.21	0.025	0.004	0.198
α-Phase[a]	Bal.	23.5	4.8	3.5	1.0	–	–	–	–	–	–
γ-Phase[a]	Bal.	20.5	7.2	1.0	2.0	–	–	–	–	–	–

[a] Energy dispersive spectrometer (EDS).

3. Results and discussion

3.1. Morphologies of etched 2205 DSS

Selective micro-etching yields a concave/convex surface on 2205 DSS. Fig. 3(a) presents some SEM micrographs of the steel after it is held at the peak potential to dissolve selectively the γ phase in the mixed 2 M H_2SO_4 + 0.5 M HCl solution for various periods. At the characteristic potential, the γ phase was selectively dissolved, leaving α phase extruding on the surface. Increasing the etching time increased the depth of the dissolved γ phase, as shown in Fig. 3(b). Notably, however, α phase was also dissolved, but at a much lower rate which was negligible. The etching depth between α and γ phases was determined from the SEM cross-sectional micrograph. In the mixed 2 M H_2SO_4 + 0.5 M HCl solution at the potential for selective dissolution of the γ phase, the etch depth increased almost linearly with time, as plotted in Fig. 4. The mean rate of the etching step between α and γ phase was about 1.9 μm h^{-1}. A depth of around 8 μm was obtained after 4 h etching. The associated increase in the surface area (in percentage) after 4 h of etching was approximately 200% of the original surface. Similar results were obtained when α phase was selectively

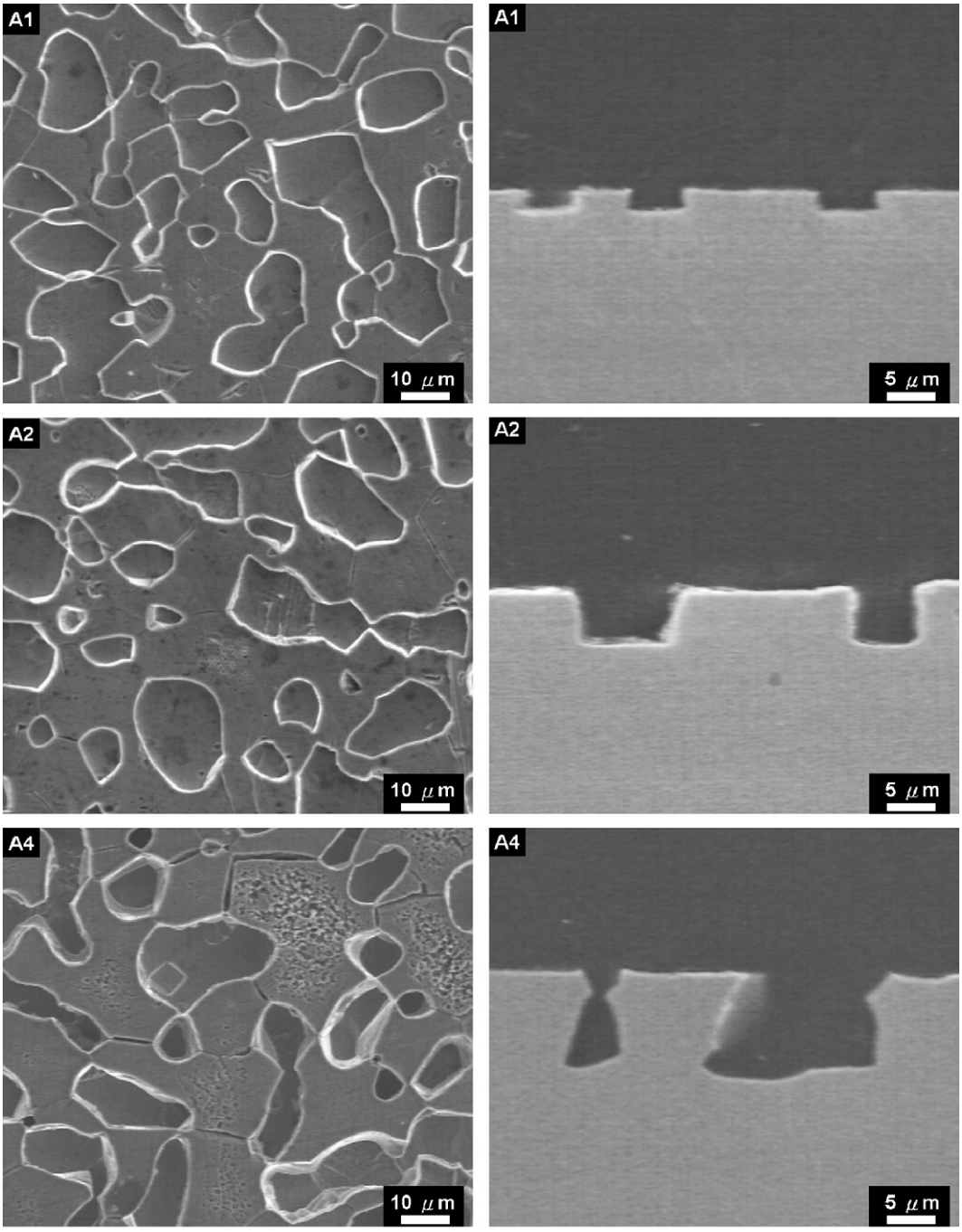

Fig. 3. (a) SEM micrographs of surface morphologies of 2205 DSS following selective dissolution of austenite phase at peak potentials for 1, 2 and 4 h; (b) corresponding cross-sectional micrographs that show increased etching depth with time.

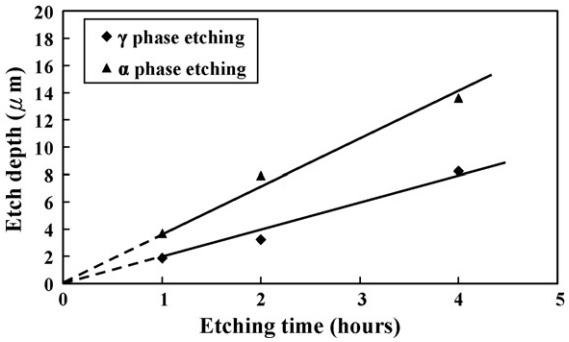

Fig. 4. Variation of etching depths with time for α and γ phases.

dissolved, leaving the extruded γ phase on the surface. The variation of the etch depth of α phase with time was also plotted in Fig. 4. Notably, however, the mean dissolution rate of the α phase was higher than that of the γ phase, and the mean etching rate at −320 mV was about 3.1 μm h^{-1}. The difference of the etching rate between γ and α phase was associated mainly with the differences between chemical compositions and applied etching potentials. Fig. 5 compares the SEM micrographs of the surface morphologies and cross-sectional images of 2205 DSS with preferential dissolution in the γ phase (Fig. 5a and c) and in the α phase (Fig. 5b and d) for 4 h. In each case, a concave/convex surface feature was observed.

3.2. Deposition of manganese oxides

Manganese oxide was deposited onto the smooth (flat and unetched) and the etched 2205 DSS by anodic electroplating. Fig. 6(a) and (b) display the surface SEM micrographs of a smooth 2205 DSS and that etched at −320 mV (with α phase preferentially dissolved), both coated with manganese oxide. Previous works have demonstrated that the thickness of oxide formed on a flat surface is approximately 500 nm when an electrical charge of 0.2 C was applied [14,15]. Since the oxide is so thin, the characteristic feature of the smooth and the etched 2205 DSS surface is still observed. At higher magnification, the manganese oxides formed on the γ and α phases, as presented in Fig. 6(c) and (d), respectively, could be clearly seen. As shown in these SEM micrographs, whisker or needle-shaped fine oxides with a nanoscale diameter were formed on the surface. Since the total surface area of the etched specimen was greater that that of the smooth one, the manganese oxide deposited at the same amount of electrical charge (0.2 C) should be thinner and might not be sufficient to completely cover the whole etched surface. Similar results were found when oxide was coated on the substrate that was pre-treated to dissolve selectively the γ phase.

The physical and chemical nature of the oxides deposited onto the etched 2205 DSS surface was further elucidated by XPS. Fig. 7 presents typical XPS spectra of deposited manganese oxide. Fig 7(a), (b) and (c) displays the spectra of the O 1s, $Mn2p^{3/2}$ and Mn3s orbits, respectively. In Fig. 7(a), the O 1s spectrum of the deposited manganese oxide obtained can be de-convoluted into

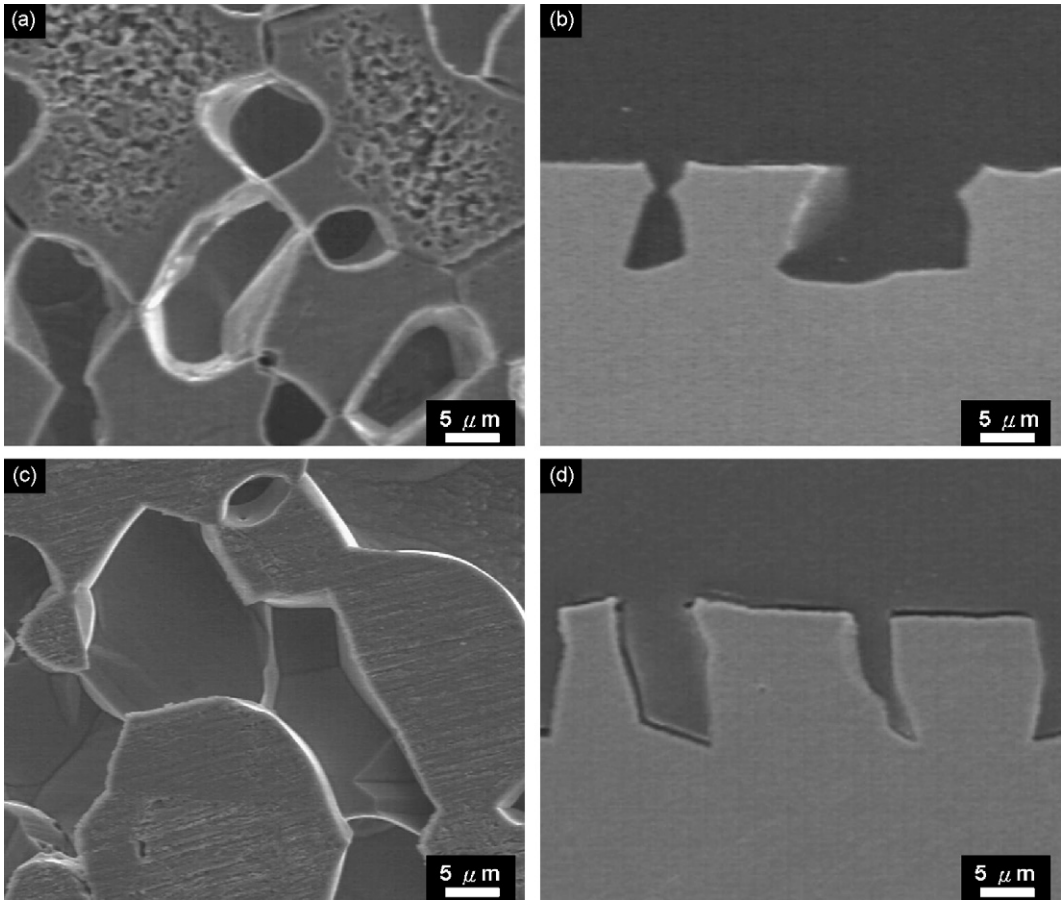

Fig. 5. SEM micrographs of surface morphologies (a) and (c), and cross-sectional images (b) and (d) of selective dissolution of γ phase at −260 mV for 4 h, and α phase at −320 mV for 4 h.

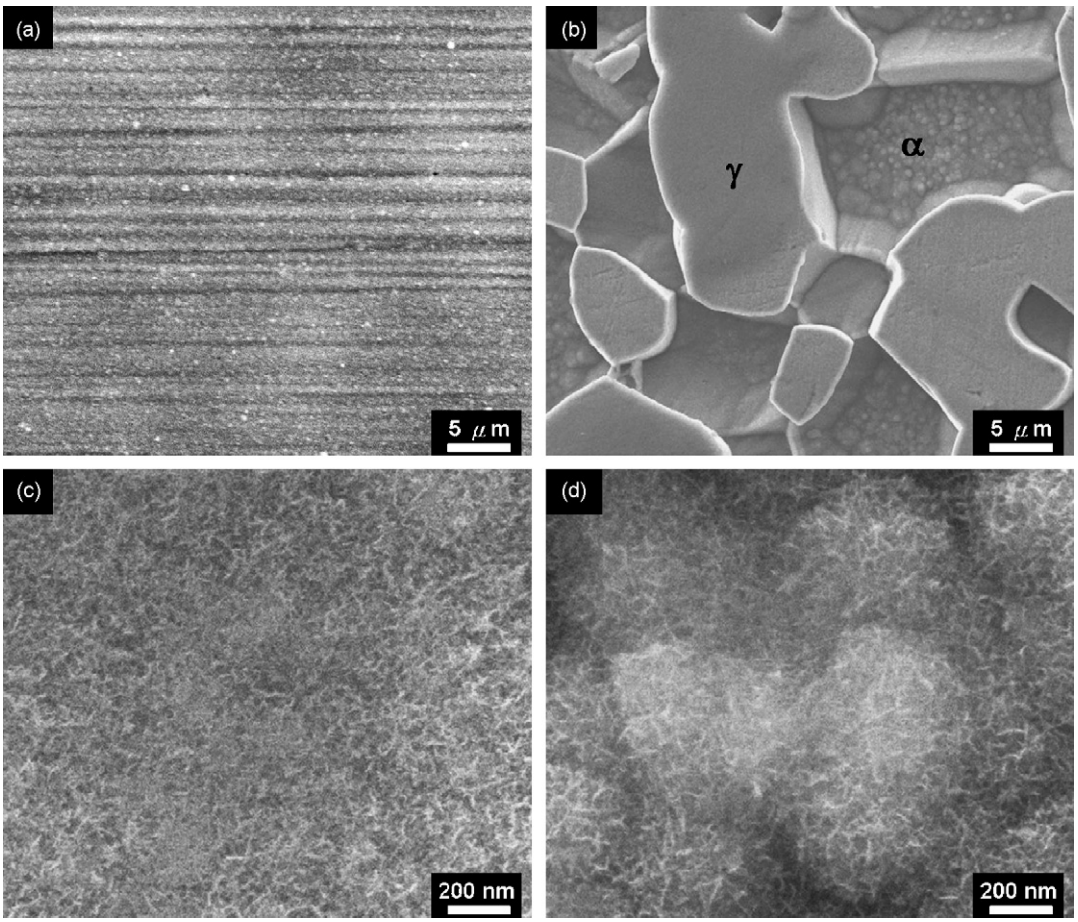

Fig. 6. SEM micrograph of manganese oxide deposited on 2205 DSS (a) smooth surface, (b) pre-etched by selective dissolution of α phase at −320 mV for 4 h; and high-magnification images of manganese oxide formed on (c) convex γ phase, and (d) concave α phase.

three constituents that correspond to different oxygen-containing species—Mn–O–Mn at 529.3–530.3 eV, Mn–O–H at 530.5–531.5 eV, and H–O–H at 531.8–532.8 eV [16,17]. Fig. 7(b) depicts the $Mn2p^{3/2}$ spectrum of deposited manganese oxide. This spectrum had a peak at a binding energy of 642.2 eV. The binding energies of the $Mn2p^{3/2}$ electron for Mn^{3+} and Mn^{4+} are 641.6 and 642.6 eV, respectively [18]. The variation of the manganese valence state can be determined more specifically by investigating the multiple splitting width of Mn3s peaks [16,17]. Fig. 7(c) shows the XPS spectrum of the Mn3s orbit of the deposited manganese oxide. Chigane and Ishikawa [16,17] reported the peak separations (ΔEs) of Mn3s for MnO, Mn_3O_4, Mn_2O_3, and MnO_2 as 5.79, 5.50, 5.41 and 4.78 eV, respectively. In this investigation, the peak separation (ΔE) was 5.24 eV. The analytic results in Fig. 7 show that these oxides comprised trivalent and tetravalent manganese oxides and water. The XPS results for the manganese oxides deposited onto 2205 DSS did not vary with the etching process.

3.3. Cyclic voltammetry and specific capacitance

Cyclic voltammograms of various electrodes were measured in 0.1 M Na_2SO_4 solution at room temperature at various potential scan rates (5, 20, 50, and 100 mV s^{-1}). Fig. 8 plots the CV curves at a potential scan rate of 20 mV s^{-1}. The CV curves of the deposited manganese oxides coated on 2205 DSS pre-etched for selective dissolution of γ (Fig. 8a) for various periods, were close to rectangular and had mirror-image characteristics. These results show the excellent reversibility and ideal pseudo-capacitive behavior of the electrodes. The specific capacitance (C) of the manganese oxides can be estimated as

$$C = \frac{\text{specific voltammetric charge}}{\text{potential range}}$$

Similar results, but with different specific capacitances, were obtained at other potential scan rates. The specific as well as the percentage increases of capacitances of various electrodes, measured at CV scan rates of 5, 20, 50 and 100 mV s^{-1}, are presented in Table 2. The increase in specific capacitance was mainly attributed to the increase in surface area.

For the specimens pre-etched for selective dissolution of α phase, the CV curves are manifested in Fig. 8(b). As shown in this figure, the CV curves for F0 (smooth) and F1 specimens exhibited ideal pseudo-capacitive behavior. However, for specimens F2 and F4, irreversible anodic peaks were seen in the potential around 0.8–1.0 V. As mentioned above, the oxide deposited under an electrical charge of 0.2 C might not be sufficient to cover the whole etched surface completely. Though stainless steel can be easily passivated in aqueous solution, passive film breakdown in the spots not coated with manganese oxide may occur at high anodic polarization condition. The irreversible peaks found for F2 and F4 specimens could be contributed from the steel substrate not covered with manganese oxide at such higher anodic polarization condition. However, the pseudo-capacitive behavior was still observed for either F2 or F4 in the potential range from 0 to 0.8 V. The specific capacitances for the electrodes prepared from the substrate pre-etched with selective dissolution of α phase, measured in the

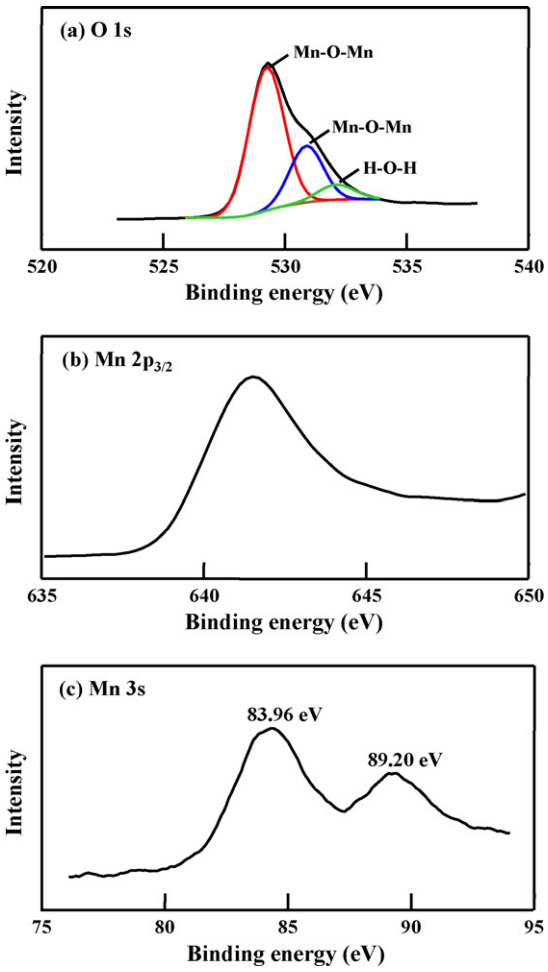

Fig. 7. XPS spectra of (a) O 1s, (b) $Mn2p^{3/2}$ and (c) Mn3s orbits for manganese oxide formed on etched 2205 DSS surface.

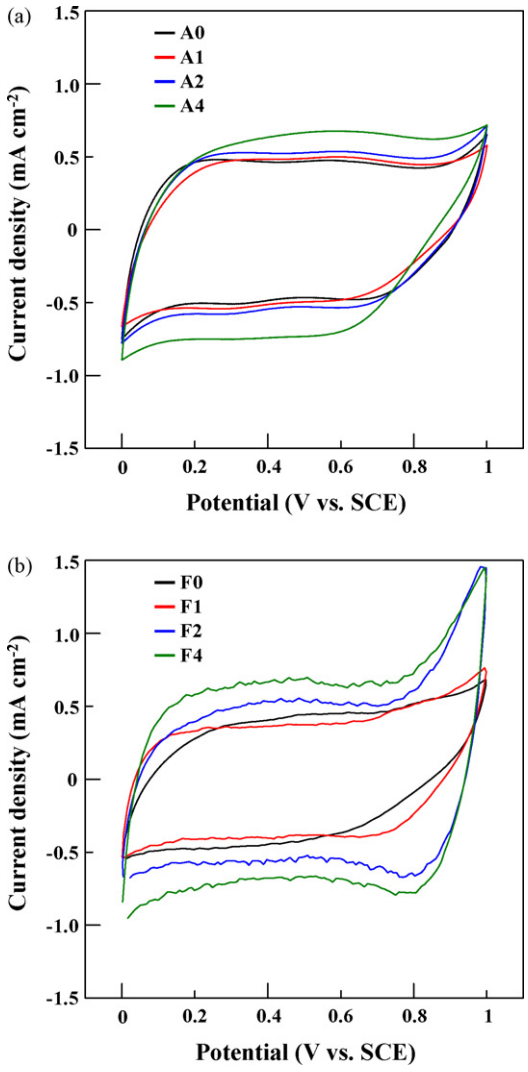

Fig. 8. Cyclic voltammograms of manganese oxides coated on 2205 DSS etched for selective dissolution of (a) γ phase and (b) α phase, in 0.1 M Na_2SO_4 solution at room temperature and at a potential scan rate of 20 mV s^{-1}.

potential range from 0 to 0.8 V and at CV scan rates of 5, 20, 50 and 100 mV s^{-1}, are presented in Table 3. The dependence of the specific capacitance on the electrode surface area, similar to that shown in Table 2, is again demonstrated.

Fig. 9 shows the effects of potential scan rate and substrate etching on the apparent specific capacitance. The specific capacitance (measured from 0 to 1.0 V) of the electrodes with pre-etched γ phase (Fig. 9a) decreased as the potential scan rate increased. The scan rate-dependent behavior was similar to that observed elsewhere. [14,19] The results revealed that at a particular scan rate, the capacitance increased with the etching depth of the γ phase. Although the specific capacitance slightly decreased with 1 h pre-etching, it increased as the etching time exceeded 2 h. The specific capacitance of the electrode pre-etched for 1 h was low probably because of the partial passivation of the surface, which gave rise to a higher electrical resistance at the oxide/metal interface. With prolonged etching, extensive metal dissolution removes the passive film. Therefore, the electrical resistance at the oxide/metal interface is reduced, and the specific capacitance increases with the surface area. The beneficial effect of a higher surface area in enhancing the capacitance is thus demonstrated in Fig. 9.

Fig. 9b reveals that the effect of etching depth, and more specifically the surface area, on the capacitance was more pronounced

Table 2
The specific capacitance and its change (in percentage) of various manganese oxides, coated on 2205 DSS substrate with γ phase selectively dissolved for different periods of time, in 0.1 M Na_2SO_4 solution and at various CV scan rates.

Scan rate (mV s^{-1})	Specific capacitance[a] (F g^{-1})/percentage change (%)							
	Specimen A0		Specimen A1		Specimen A2		Specimen A4	
	F g^{-1}	%	F g^{-1}	%	F g^{-1}	%	F g^{-1}	%
5	182	–	175	−4	190	4	204	12
20	145	–	141	−3	147	1	163	12
50	125	–	121	−3	126	1	133	6
100	110	–	105	−5	112	2	115	5

[a] Determined in the potential range of 0–1.0 V.

Table 3
The specific capacitance and its change (in percentage) of various manganese oxides, coated on 2205 DSS substrate with α phase selectively dissolved for different periods of time, in 0.1 M Na_2SO_4 solution and at various CV scan rates.

Scan rate ($mV\,s^{-1}$)	Specific capacitance[a] ($F\,g^{-1}$)/percentage change (%)							
	Specimen F0		Specimen F1		Specimen F2		Specimen F4	
	$F\,g^{-1}$	%	$F\,g^{-1}$	%	$F\,g^{-1}$	%	$F\,g^{-1}$	%
5	132	–	127	−4	162	23	209	58
20	103	–	105	2	141	37	184	79
50	76	–	89	17	133	75	163	114
100	56	–	77	38	126	124	149	166

[a] Determined in the potential range of 0–0.8 V.

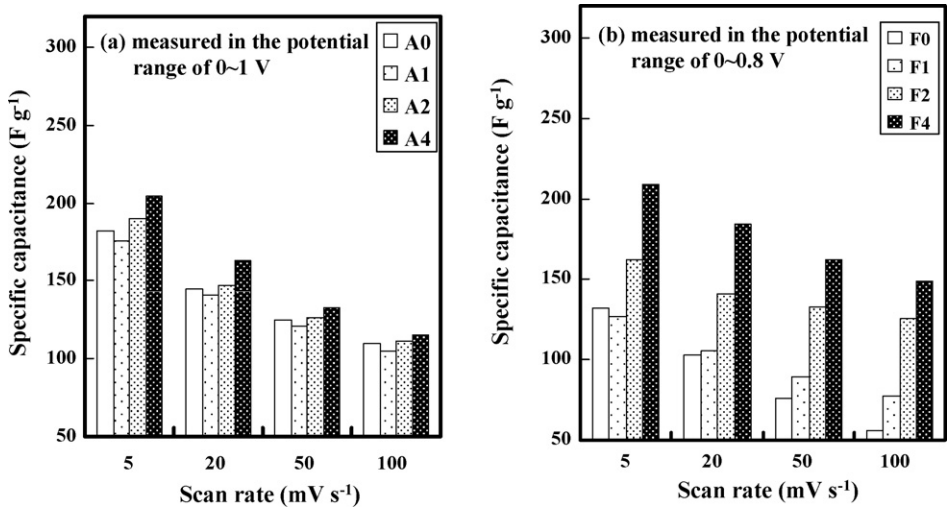

Fig. 9. Comparison of specific capacitances of manganese oxides coated on 2205 DSS substrates with pre-etched (a) γ phase, and (b) α phase to various depths, in 0.1 M Na_2SO_4 solution at room temperature and at various potential scan rates.

than that displayed in Fig. 9a, especially with regard to the percentage increase in capacitance. It should be pointed out that the specific capacitances were measured in the potential range of 0–0.8 V. At a scan rate of $5\,mV\,s^{-1}$, for instance, the capacitance of the F4 electrode was $209\,F\,g^{-1}$, which was approximately 58% greater than that of the F0 electrode ($132\,F\,g^{-1}$). As shown in Table 3, an even higher increase (about 166%) in specific capacitance was observed at a scan rate of $100\,mV\,s^{-1}$ for F4 electrode. As stated above, the rate of selective dissolution in α phase was greater than that in γ phase at their respective peak potentials. Accordingly, the increase in the surface area was higher for electrodes F1, F2 and F4 than for A1, A2 and A4. Consequently, the increase in specific capacitance became appreciable upon pre-etching of the substrate with selective dissolution of α phase, as can be seen by comparing the results shown in Tables 2 and 3.

4. Conclusions

Constituent phases selectively dissolved in 2205 DSS in 2 M H_2SO_4 + 0.5 M HCl solution at specific characteristic potentials. Micro-etching was thus adopted to fabricate the electrode substrate with a concave/convex surface with a high surface area. The etch depth resulting from selective dissolution increased with etching time. The etching rate of the α phase exceeded that of the γ phase at the respective characteristic potentials. Manganese oxide was successfully deposited on the micro-etched 2205 DSS substrate. The specific capacitance of the manganese oxide electrode was greatly enhanced by exploiting the selectively micro-etched 2205 DSS substrate. The increase in specific capacitance was greater for the electrode where selective dissolution occurred in the α phase.

Acknowledgement

The authors would like to thank the National Science Council of the Republic of China, Taiwan, for financially supporting this research under Contract no. NSC 94-2216-E-006-020.

References

[1] C.C. Hu, T.W. Tsou, Electrochem. Commun. 4 (2002) 105–109.
[2] C.C. Hu, T.W. Tsou, Electrochim. Acta 47 (2002) 3523–3532.
[3] J.K. Chang, C.T. Lin, W.T. Tsai, Electrochem. Commun. 6 (2004) 666–671.
[4] S.C. Pang, M.A. Anderson, T.W. Chapman, J. Electrochem. Soc. 147 (2000) 444–450.
[5] J.K. Chang, W.T. Tsai, P.Y. Chen, C.H. Huang, F.H. Yeh, I.W. Sun, Electrochem. Solid-State Lett. 10 (2007) A9–A12.
[6] T. Shinomiya, V. Gupta, N. Miura, Electrochim. Acta 51 (2006) 4412–4419.
[7] T. Xue, C.L. Xu, D.D. Zhao, X.H. Li, H.L. Li, J. Power Sources 164 (2007) 953–958.
[8] I.H. Lo, Y. Fu, C.J. Lin, W.T. Tsai, Corros. Sci. 48 (2006) 696–708.
[9] W.T. Tsai, J.R. Chen, Corros. Sci. 49 (2007) 3659–3668.
[10] J.P. Zheng, T.R. Jow, J. Electrochem. Soc. 142 (1995) L6–L8.
[11] J.P. Zheng, P.J. Cygan, T.R. Jow, J. Electrochem. Soc. 142 (1995) 2699–2703.
[12] Y. Takasu, T. Nakamura, H. Ohkawauchi, Y. Murakami, J. Electrochem. Soc. 144 (1997) 2601–2606.
[13] J. Wei, N. Nagarajan, I. Zhitomirsky, J. Mater. Process. Technol. 186 (2007) 356–361.
[14] J.K. Chang, W.T. Tsai, J. Electrochem. Soc. 150 (2003) A1333–1338.
[15] J.K. Chang, W.T. Tsai, J. Electrochem. Soc. 152 (2005) A2063–2068.
[16] M. Chigane, M. Ishikawa, J. Electrochem. Soc. 147 (2000) 2246–2251.
[17] M. Chigane, M. Ishikawa, M. Izaki, J. Electrochem. Soc. 148 (2001) D96–D101.
[18] B.R. Strohmeier, D.M. Hercules, J. Phys. Chem. 88 (1984) 4922–4929.
[19] J.K. Chang, Y.L. Chen, W.T. Tsai, J. Power Sources 135 (2004) 344–353.